Case Studies in Construction Materials 25 (2026) e06244

Contents lists available at ScienceDirect

Case Studies in Construction Materials

journal homepage: www.elsevier.com/locate/cscm

Understanding the reactivity of biomass ash from a pulverised fuel combustor

Ivana Carević [a], Marijana Serdar [a], Vilma Ducman [b], Sabina Dolenec [b,c], Maruša Mrak [b], Nina Štirmer [a,*]

[a] University of Zagreb Faculty of Civil Engineering, Department of Materials, Fra Andrije Kačića Miošića 26, Zagreb 10000, Croatia
[b] Slovenian National Building and Civil Engineering Institute, Dimičeva ulica 12, Ljubljana 1000, Slovenia
[c] University of Ljubljana, Faculty of Natural Sciences and Engineering, Aškerčeva ulica 12, Ljubljana 1000, Slovenia

ARTICLE INFO

Keywords:
Wood ash
Biomass ash
Reactivity
Microstructure
SCM
Blended cements

ABSTRACT

The manuscript provides long-term microstructural study on as-collected wood biomass ash (WBA) from a pulverised fuel combustor. Analytical methods, including isothermal calorimetry, X-ray powder diffraction, thermogravimetric analysis, and mercury intrusion porosimetry, were used to assess reaction kinetics, phase development, and porosity. Results show that WBA increases water demand due to its irregular particle morphology and high content of unburnt carbon and carbonates, causing a dilution effect that delays hydration reactions and extends the induction period. Microstructural analysis revealed significant changes in porosity, with an increase in pores between 0.01–0.05 μm during early hydration. As a result, early mechanical strength is reduced. Over time, the pozzolanic activity and carbonation of WBA enhance compressive strength, improving long-term performance. The study highlights the potential of WBA as a sustainable cement substitute and emphasises the need for further research to optimise its integration into concrete applications and assess its durability in various environments.

1. Introduction

The use of supplementary cementitious materials (SCMs) in the cement and concrete industry is the most practical and economical method for reducing CO_2 emissions and conserving natural resources, both of which have a positive impact on the environment [1]. The utilization of various wastes or by-products from other industrial streams, such as slag, coal fly ash, and others, is widely used in the cement and concrete industry, where circularity and material efficiency of these secondary raw materials are integrated and firmly established through industrial symbioses [2]. Each SCM in a concrete mixture influences the formation of hydration products: a hydraulic material sets and hardens under water, while pozzolans need calcium hydroxide (portlandite, $Ca(OH)_2$) and water to produce hydrates. Pozzolanic and hydraulic reactivity and the type and properties of the phases formed during these reactions are parameters that need to be evaluated when cement is replaced by a novel SCM. Changes in hydration products are followed by changes in pore structure [3,4], consequently leading to changes in durability and mechanical properties. Understanding microstructural development in the blended system is important to optimize the use and the replacement levels of SCMs [5].

In recent years, research on the application of wood biomass ash (WBA) as SCM in the construction sector has intensified [6–17]. WBA exhibit varying characteristics and properties when used as a partial cement replacement [18,19]. In a number of studies, the

* Corresponding author.
E-mail address: nina.stirmer@grad.unizg.hr (N. Štirmer).

https://doi.org/10.1016/j.cscm.2026.e06244
Received 5 March 2026; Received in revised form 19 May 2026; Accepted 15 June 2026
Available online 16 June 2026

effects of WBA on cementitious composites are attributed to the pozzolanic properties [20–23], while in other studies to the hydraulic properties [20,24–26] and/or a lack of pozzolanic properties [12]. Where detected, pozzolanic activity of WBA is attributed to the high content of silicon, iron oxides, aluminium, or amorphous silica [21,22]. On the other side, when the lack of pozzolanic activity was detected, it was explained by the limited silicon content [11,12]. In certain studies, hydraulic activity of WBA was observed, noting its ability to react directly with water and form cementitious phases without activation [24,27]. Variations in the effect of WBA on the properties of cement composites observed in the literature are mostly due to differences in the type of biomass, combustion technology and temperature used in the plant, location of WBA collection, and storage of WBA [18]. In most of the studies investigating the effect of cement replacement with WBA, regardless of the source and combustion technology used to obtain WBA, replacing 5–10% of cement with WBA did not significantly affect the workability of cementitious materials and did not have negative influence on mechanical properties [8,28,29]. Results show that with a higher proportion of WBA used as SCM, a reduction in compressive strength can be expected [8,10,30,31]. WBA addition enhances durability properties more significantly than mechanical properties. This improvement is attributed to their pore-filling effect, which leads to the densification of the cementitious microstructure [28].

Previous studies on the microstructure of Portland cement with WBA from grate combustion showed an increased amount of bound water, ettringite, and calcite, and a decreased amount of portlandite in all pastes with WBA compared to the Portland cement reference [24]. During early-age hydration, when WBA from grate combustion is used, a large amount of portlandite can be expected due to higher levels of reactive CaO. However, after some time, portlandite is consumed as a result of the activated pozzolanic reaction [20, 32]. The incorporation of WBA reduces the mean pore size, with a more pronounced effect at higher replacement ratios compared to the reference mixture [33]. Hydration kinetics decrease with increasing cement replacement levels due to lower reactivity [32,33]. While WBA obtained from grate combustion is to certain extent researched, there is limited understanding and consensus of the long-term changes in kinetics and microstructural development of cement composites when WBA from pulverised fuel combustion replaces part of the Portland cement. Pulverised fuel combustor technology involves milling of biomass to fractions smaller than 1 mm and feeding those fractions into the combustion zone through special burners as dispersed fuel particles. This process differs from grate or fluidized bed combustion [34,35], leading to significant differences in chemistry and microstructure of obtained WBA. Chemical and microstructural changes of WBA from pulverised fuel combustion, compared to WBA from grate combustion, are important because they can modify the microstructure and change the long-term properties of cementitious composites [27].

The manuscript provides a long-term (1-year), multi-technique microstructural study on as-collected WBA from a pulverised fuel combustor, a system distinct from the more commonly studied fluidized bed and grate combustion. To understand the long-term effect of this specific WBA on the microstructure of cement composite, cement pastes and mortar with 15 wt% cement replaced by WBA were prepared and systematically analysed over the long term (up to 1 year), using various analytical techniques such as isothermal calorimetry, X-ray powder diffraction (XRD), thermogravimetric analysis, and mercury intrusion porosimetry. The results of the analytical techniques were used to reveal the dominant early-age and long-term effects of WBA from pulverised fuel combustors on the properties of cementitious composites.

2. Materials and methods

2.1. Characterization of raw materials

WBA was collected from a power plant using pulverized fuel combustor technology and was subsequently characterized. The

Table 1
Chemical analysis and physical characteristics of WBA and OPC (wt%).

Chemical analysis (wt%)		
	WBA	**OPC**
CaO	51.90	59.80
SiO_2	9.28	21.88
Al_2O_3	2.28	4.94
SO_3	3.58	3.33
Fe_2O_3	1.47	3.15
MgO	3.75	2.01
K_2O	9.20	1.25
Na_2O	0.55	0.85
TiO_2	0.15	0.23
P_2O_5	1.84	0.22
Na_2O_{eq}	6.60	1.67
$SiO_2+Al_2O_3+Fe_2O_3$	13.03	29.97
Free CaO	13.50	2.50
Free MgO	3.80	0.75
LOI (950 °C)	13.80	3.60
pH	13.25	12.86
Density (g/cm^3)	2.59	3.10
Bulk density (g/cm^3)	0.38	n/a
d_{50} (μm)	43.30	9.60
% passing 21.23 μm sieve	14.50	70.40

chemical composition of the WBA was analyzed according to EN ISO 16967 [36]. pH values were determined following EN 12176 [37] The European Committee for Standardization, Charact. Sludge – Determ. pH-Value (EN 12176 1998.The European Committee for Standardization. Characterization of sludge – Determination of pH-value (EN 12176:1998) 1998.[37], and the loss on ignition (LOI) was measured according to ASTM D7348–13 [38]. Density was determined using the Le Chatelier flask method in accordance with ASTM C188 [39]. Free CaO content was evaluated according to EN 451–1 [40]. The morphology of the WBA samples was examined using scanning electron microscopy (SEM) with a FE MIRA II LMU instrument, operated in high vacuum mode at a pressure of (30–50)$\times$ 10^{-3} Pa and an accelerating voltage of 10 kV. Before imaging, the samples were sputter-coated with a thin layer of gold/-palladium (Au/Pd) in argon (Ar) plasma. The particle size was analysed using a Sympatec HELOS/BF-MAGIC laser diffraction analyser. Samples were dispersed in an air stream at a pressure of 0.2 MPa, and the results were interpreted using the Fraunhofer approximation.

X-ray powder diffraction analysis was performed on a PANalytical Empyrean X-ray diffractometer equipped with CuKα radiation with $\lambda = 1.54$ A at 45 kV and a current of 40 mA. Powder samples were back-loaded into a circular sample holder (diameter 27 mm) to avoid the preferred orientation effects. Samples were measured in a range of 5–100 ° 2θ with a step size of 0.026 °2θ using a 1° divergence slit and a 15 mm mask. The external standard NIST 676a (alumina powder Al_2O_3) was used to determine the amount of amorphous phase. PANalytical's X'Pert High Score Plus v. 4.9 diffraction software was used to analyse the diffraction patterns and refinements with the Rietveld method, using structures for the phases from the ICDD PDF 4 + 2020 RDB powder diffraction files and publication references.

WBA is generated in a power plant using pulverised fuel combustor technology, where mainly beech, oak, hornbeam, and mixed wood are burned at an average temperature of 700–750 °C. The chemical and physical properties of WBA and ordinary Portland cement (OPC), CEM I 42.5 R as well as their particle size distribution, morphology, and phase composition, are presented in Table 1, Table 2, and Fig. 1. WBA exhibited significantly higher values of sodium oxide equivalent (Na_2Oeq), free calcium oxide (free CaO), and loss on ignition (LOI) compared to OPC. Specifically, the Na_2Oeq content in WBA was 6.60%, while in OPC it was 1.67%. The free CaO content in WBA reached 13.50%, whereas OPC contained only 2.50%. Similarly, the LOI measured at 950 °C was 13.80% for WBA and 3.60% for OPC.

The mineralogical composition of WBA differs significantly from that of OPC, with a prevalence of non-clinker phases. In WBA, calcite (33.7%) and portlandite (26.6%) are predominant, along with a notable amount of amorphous phase (22.3%), indicating the presence of carbonate and hydrated products and suggesting potential reactivity. β-Belite (6.4%), arcanite (K_2SO_4, 5.7%), quartz, and periclase are also present, while the content of free (unbound) lime is low (0.4%). In contrast, OPC contains a high proportion of clinker phases, with alite (59.8%), β-belite (8.5%), ferrite (8.2%), and aluminate (4.3%), which accounts to its hydraulic reactivity. The amorphous phase in OPC is only 8.3%, considerably lower than in WBA. Calcite (7.4%) and periclase (0.4%) are present in smaller amounts, while trace amounts of anhydrite and gypsum play a role in setting regulation.

SEM micrographs of WBA reveal irregular particle morphology and heterogeneous surface texture. Particle size distribution data show that WBA has a significantly coarser grain structure than OPC. The irregular shape and coarser texture of WBA may reduce packing efficiency and increase water demand, influencing workability and potentially reactivity.

2.2. Cement paste and mortar sample preparation

Analyses were performed on cement pastes and mortars. The reference cement paste and mortar were designated as P0 and M0, respectively, while samples with 15% cement replaced by WBA were designated as P1 (cement paste) and M1 (mortar).

Microstructural analysis was performed on two cement pastes (P0 and P1), both prepared in accordance with EN 196–3 [41]. The reference paste (P0) was made using 500 g of CEM I 42.5 R and 125 g of water, corresponding to the standard consistency. For paste P1, where WBA was incorporated as a partial cement replacement, the water content was adjusted to achieve standard consistency. Specifically, for paste P1 166 g of water per 500 g of binder was required. Paste samples with dimensions 4 × 4 × 16 cm were prepared, with three specimens per mix, and their compressive strength was tested at 7, 28, and 90 days in accordance with EN 196–1 [42].

Mortar samples of the reference mix (M0) and the mix with 15% cement replaced by WBA (M1) were used to determine compressive strength at 7, 28, 90 and 365 days. The mortars were prepared with a mass ratio of CEN standard sand, CEM I 42.5 R and

Table 2
Phase composition of WBA and OPC as determined by X-ray powder diffraction and Rietveld analysis (wt%).

Phase composition (wt%)			
	WBA		**OPC**
Calcite	33.7	**∑Alite**	59.8
Portlandite	26.6	**β-Belite**	8.5
β-Belite	6.4	**Ferrite**	8.2
Arcanite	5.7	**Aluminate**	4.3
Quartz	3.7	**Gypsum**	2.0
Periclase	1.2	**Calcite**	7.4
Lime	0.4	**Dolomite**	0.6
Anhydrite	0.1	**Quartz**	0.5
Amorphous	22.3	**Periclase**	0.4
		Amorphous	8.3

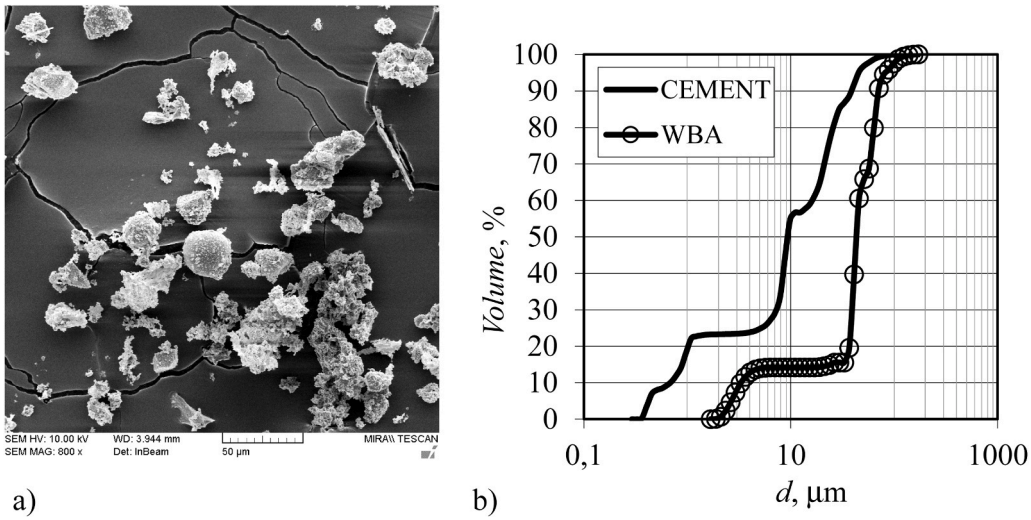

Fig. 1. a) Morphology of the WBA sample obtained by SEM/SE; at 800x magnification, b) Particle (volume)-size distribution of WBA and cement samples.

water of 3:1:0.5 and a w/c 0.5 in accordance with EN 196–1 for compressive strength testing [42].

2.3. Methods

After mixing, various fresh properties of both pastes and mortars were evaluated (consistency, setting times, soundness, temperature, density, air content, and flow consistency), as detailed in the previous publication [8].

The heat of hydration and cumulative heat of the reference cement paste (P0) and cement with WBA (P1) were analysed by isothermal calorimetry using a TAM calorimeter (TA instruments), with water-binder ratio of 0.5. Approximately 20 g of each sample was mixed ex-situ for 3 min, and 6 g of the sample was placed in a sealed vial and lowered into the calorimeter. The heat evolution of the cement was evaluated for 7 days at 20 °C.

After casting the cement pastes, test specimens were covered with plastic sheets to prevent water evaporation and stored for up to 24 h under laboratory conditions (relative humidity about 60% and temperature of 20 °C). They were then stored in a chamber at a relative humidity above 95% and a temperature of 20 °C until the day of testing. Cement paste samples were first used for mechanical tests, after which smaller fragments of the sample were taken for microstructural analysis. Before microstructural analysis, the samples were immersed in isopropanol for 24 h, vacuumed for 8 h and dried in an oven at 40 °C for 24 h to stop hydration and remove free waster [43]. Oven drying removes free water efficiently but may also remove structural water, leading to the decomposition of ettringite and AFm phases [44]. However mild the oven drying used in the study, there remains a risk that the chosen drying method influenced the results of the phase assemblage obtained. This applies to each method of hydration stoppage, whether based on drying or solvent exchange. Therefore, phase assemblage results in this study should be compared with results where hydration was stopped using the same procedure, to ensure that changes in phase assemblage are due to WBA addition and not the hydration stoppage procedure itself.

After hydration stoppage, fragments of the paste sample were used for MIP testing. Other fragments were ground to below 0.063 mm to obtain a fine powder for TGA and XRD analysis. After grinding and before testing, fragments and powdered samples were sealed in plastic foil and stored in plastic containers. Even though the samples were dried and sealed in plastic foil and plastic containers, and tests were performed as soon as possible depending on equipment availability, the possibility that the powdered samples carbonated cannot be fully excluded.

Thermogravimetric analysis (TGA) of the pastes with WBA (P1) and the reference sample (P0) was carried out using a NETZSCH STA 409 PC/PG in an alumina crucible filled with approximately 30 mg of powder sample. The temperature measurement interval for all samples was 25 °C to 1200 °C, with a heating rate of 10 °C/min. The sample chamber was filled with inert gas (nitrogen, flow rate: 30 mL/min) to prevent oxidation during measurement. The analysis of bound water (H) and the amount of portlandite (CH) were calculated according to [44,45].

$$H = \frac{W_{50} - W_{500}}{W_{500}} \tag{1}$$

where

W_{50} – weight at 50 °C

W_{500} – weight at 500 °C

$$CH = \frac{W_{400} - W_{600}}{W_{600}} \times \frac{M(Ca(OH)_2}{M(H_2O)} \quad (2)$$

where

W_{400} – weight at 400 °C

W_{600} – weight at 600 °C

M – molecular masses of water (18 g/mol) and portlandite (74 g/mol)

X-ray powder diffraction analysis of the paste samples was performed in the same as way as for the raw materials (as described in Chapter 2.1).

The pore size distribution of the samples was determined using an Autopore IV 9500 Micromeritics Mercury porosimeter. Sample fragments from each mixture, with a mass ranging from 1.4 to. 2.4 g were used.

3. Results

3.1. Hydration kinetics

Fig. 2a) shows the hydration heat flow normalized to the binder content, while Fig. 2b) shows the cumulative heat over 7 days for the reference mix (P0) and the mix with 15% WBA (P1). The addition of WBA reduced the initial heat of hydration and slightly increased the induction time, suggesting a delayed acceleration period. Similarly, the authors [46] investigated the heat of hydration of pastes with fly WBAs as a cement replacement and showed that the induction time increased with the addition of WBAs. The main hydration peak occurred at approximately 10.6 h for the reference mixture and 14.6 h for the sample with WBA. Comparison of the cumulative heat flow of the reference mixture and the sample with 15% WBA shows the influence of WBA on the heat of hydration: the cumulative heat flow at 7 days for the paste with 15 wt% WBA is almost equal to that of the reference mixture (Table 3). Cement replacement in paste P1 with WBA slightly delays early hydration (lower value in the first 24 h), but the differences decrease over time. Therefore, it can be concluded that the addition of WBA did not negatively influence the heat of hydration. On the contrary, despite significant substitution of cement by WBA, the heat of hydration remained similar, indicating reactivity of WBA.

3.2. Evolution of the mechanical properties

Fig. 3 shows the compressive strength values and standard deviation (presented as error bars) of the mortars and pastes at different ages, indicating that the mixtures with WBA (M1 and P1) have lower compressive strength than the reference mixtures (M0 and P0) at all test periods. The greatest decrease in compressive strength is observed at early ages in the WBA cement samples, which is consistent with previous studies [10]. The compressive strength at 7 days for cement paste (P1) and mortar (M1) was 21% and 25% lower than

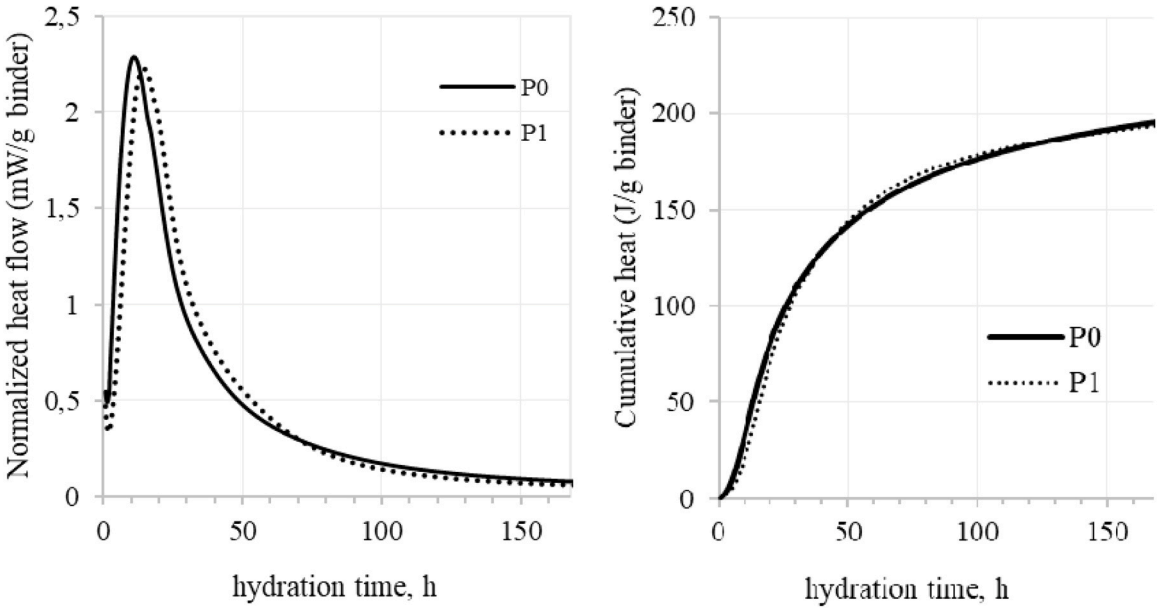

Fig. 2. a) Hydration heat flow of the reference mix (P0) and the mix with WBA (P1), normalised per mass of the binder; b) Cumulative heat of hydration of the reference mix (P0) and the mix with WBA (P1), normalised per mass of the binder.

Table 3
Cumulative heat of hydration of cement pastes P0 and P1 at different time periods, normalised per mass of the binder (J/g binder).

	Time		
Mixture	**24 h**	**72 h**	**186 h**
P0	94.6	161.3	195.1
P1	87.9	165.1	193.3

the reference mixes P0 and M0, respectively, which exceeds the percentage of cement replaced by WBA. At 28 and 90 days of hydration, the compressive strength of the M1 mix was 13% lower than the reference mix (M0), while the values for the paste (P1) were even lower (27% and 18%, respectively). Compressive strength did not change significantly between 90 and 365 days for mortar M0, while it continued to increase when WBA (M1) is added. A similar trend is observed in previous literature [30], [47], [48].

3.3. Phase composition of hydration products

Fig. 4 presents the TGA and DTG curves of the reference mixture (P0) and the mixture with 15% WBA as cement replacement (P1). Three main peaks can be identified from the TGA. The first peak occurs between 50 and 250 °C. Mass losses in the temperature range up to around 105 °C are usually attributed to the release of adsorbed and capillary water from the sample [46]. However, there are indications that many cement hydrates (especially C−S−H, ettringite, and monosulphate) lose some of their chemically bound water below 105 °C [44]. Therefore, a temperature below 50 °C is attributed to absorbed water in the sample, while a temperature above 50 °C is attributed to the decomposition of hydration products. The peak between around 100 °C was attributed to C−S−H and ettringite. According to the literature, C−S−H gel exhibits weight loss in the temperature range of approximately 50–250 °C, while ettringite decomposes with a characteristic weight loss around 120 °C [44]. Due to the overlapping temperature ranges, it may be challenging to clearly distinguish the thermal signals of C–S–H and ettringite, especially in complex systems [44]. In the present study, the second peak was visible at about 450 °C. Portlandite generally decomposes between 400 and 600°C to CaO and H_2O [46], [49], [50]. Finally, the third peak was observed at about 700 °C, and this peak was attributed to the decomposition of calcite to CaO and CO_2 [46], [49–51].

Based on these temperature ranges, Table 4 presents mass loss values for samples P0 and P1 at different temperature intervals, where the values represent the decomposition of the most abundant solids in the sample. According to Table 4, the first weight loss, related to the ettringite and C−S−H gel phases in the P1 samples, increased with longer curing times. This increase was more pronounced for the P1 mixture at the later age (7 days) than for the P0 mixture, which has already reached its maximum 7 days after curing. The second weight loss, related to portlandite, increased for the P1 sample up to 28 days of age and then decreased slightly after 90 days. The third weight loss (calcite) for P1 did not allow a clear conclusion on hydration up to 90 days, but after 1 year the values rose significantly (from 4.9% after 90 days to 9.0% after 1 year, Table 4). The same trend was observed for sample P0, but it was not as significant. The decreasing values for the first weight loss after 1 year in P1 samples can be attributed to the carbonation of ettringite and C-S-H gel, which consequently leads to an increase in the third peak (amount of carbonates). In general, the values for calcite are slightly higher for sample P1 than for sample P0 because WBA contains carbonatable minerals such as lime, portlandite, belite, and alite [52]. Additionally, a considerable amount of calcite may originate from the WBA itself (33.7% from Table 2), further contributing to the observed values in sample P1.

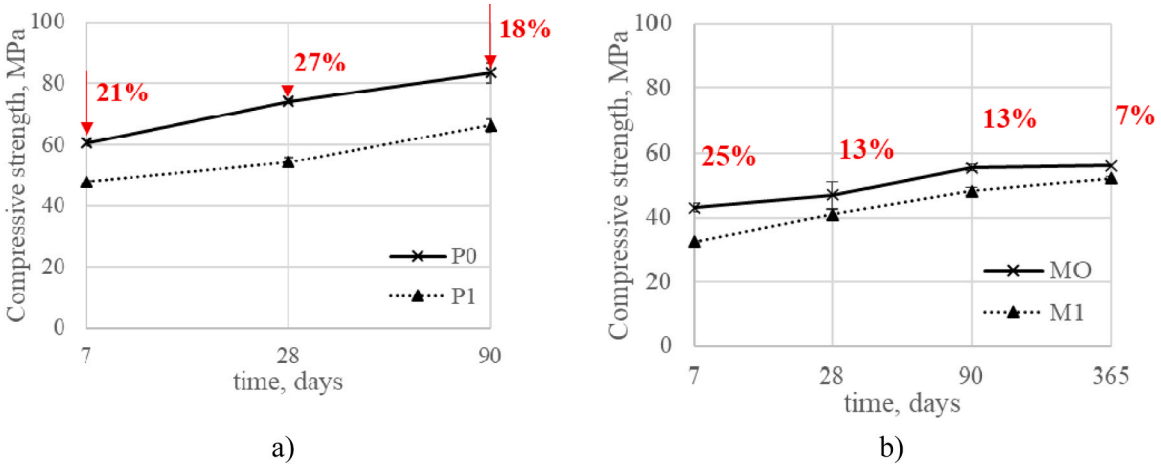

Fig. 3. Compressive strength of a) pastes and b) mortars (the red arrow indicates the percentage decrease in compressive strength of mixtures M1 and P1 compared to the reference mixtures M0 and P0).

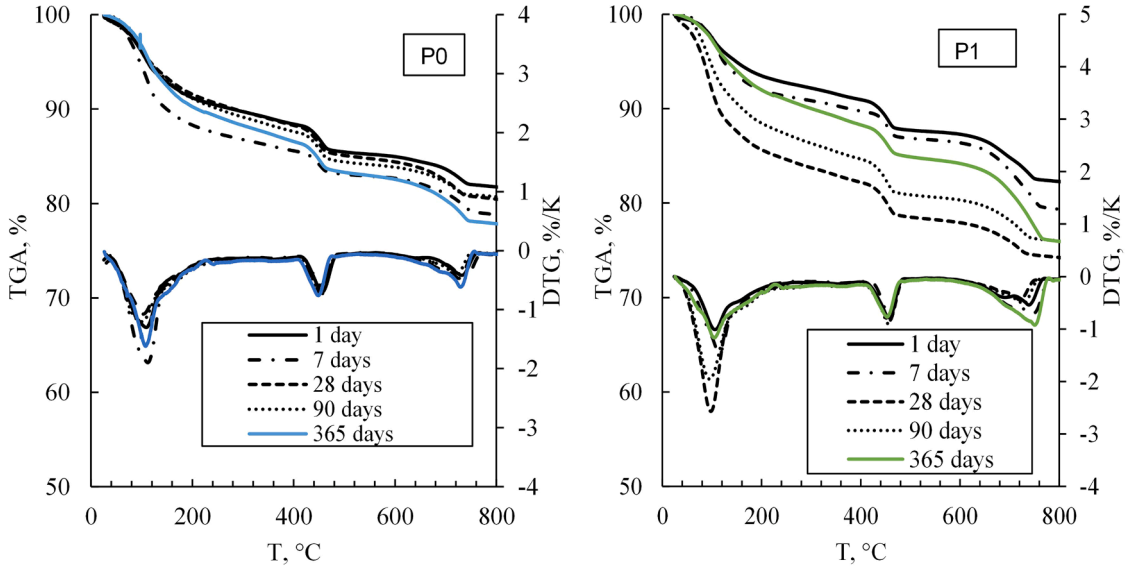

Fig. 4. TGA and DTG curves of paste P0 and P1 at 1, 7, 28, 90 and 365 days.

Table 4
Mass loss values in the temperature range (Δm) with curing time for cement paste.

Mix	Age	m_{50}	m_{400}	Δm (m_{50}-m_{400})	m_{600}	Δm (m_{400}-m_{600})	m_{950}	Δm (m_{950}-m_{600})
		%	%	%	%	%	%	%
P0	1	99.2	88.4	10.9	85.0	3.5	81.4	3.6
	7	98.9	85.6	13.5	82.7	2.9	78.4	4.2
	28	98.9	88.3	10.8	84.4	3.9	79.8	4.6
	90	99.6	87.6	12.0	83.8	3.8	80.3	3.6
	365	99.5	86.6	13.0	82.6	4.0	77.2	5.4
P1	1	99.5	90.9	8.5	87.3	3.7	81.8	5.5
	7	99.8	89.8	10.1	86.4	3.4	78.7	7.7
	28	98.6	82.2	16.6	77.9	4.3	73.6	4.3
	90	99.6	84.7	15.0	80.3	4.3	75.4	4.9
	365	99.4	88.3	11.2	84.2	4.1	75.3	9.0

X-ray powder diffraction analyses of the hydrated reference mix P0 and the sample with 15% WBA (P1) at 1, 7, 28, 90 and 365 days of age are presented in Table 5, while the diffraction patterns are shown in Fig. 5.

The X-ray powder diffraction results indicate the presence of alite, belite, aluminate, ferrite, calcite, dolomite, and quartz as unhydrated phases, and ettringite and portlandite as the main hydration products. Additionally, an amorphous phase is present in the hydrated pastes. Both calcium sulfate and periclase, present in unhydrated samples, have already reacted and are therefore not detectable after 24 h. Alite and belite content gradually decrease over time due to hydration. Alite decreases faster than belite, as belite

Table 5
Phase composition of cement pastes P0 and P1 at specified ages (wt%).

days	1		7		28		90		365	
sample/phase (wt%)	P0	P1	P0	P1	P0	P1	P0	P1	P0	P1
alite	21.1	16.1	17.2	15.9	15.7	11.8	12.9	9.8	6.3	5.6
belite	10.3	9.6	12.4	8.2	12.6	5.6	10.9	4.5	7.3	2.8
aluminate	1.3	1.4	0.7	0.8	0	0	0	0	0	0
ferrite	4.2	3.5	3.9	3.4	3.1	2.2	2.7	2	2.1	1.8
lime	/	0.2	/	0.3	/	0	/	0	/	0
portlandite	17.2	20.6	17.3	18.9	19.7	19.7	21.3	21	16.9	15.5
calcite	12.4	15.3	13.9	16.9	15	14.3	14.8	14.4	15.2	20.1
dolomite	0.7	0.9	0.7	1.1	0.7	0.9	0.9	1	0.8	0.7
quartz	0.5	1.1	0.4	1.7	0.4	0.9	0.4	1	0.3	0.6
ettringite	4.2	1.7	3.9	3.1	2.7	3.4	2.8	4	3.5	3.4
amorphous	28.1	29.6	29.5	29.7	30.1	40.5	33.3	41.7	47.6	49

is a slowly reactive phase, and a decrease in ferrite was already observed after one day. The amount of quartz was significantly higher in the samples with WBA due to the addition of WBA. The amorphous phase is mainly attributed to C−S−H, which, together with portlandite is the main product of the hydration of alite and belite. The amount of amorphous phase increased over time, which is

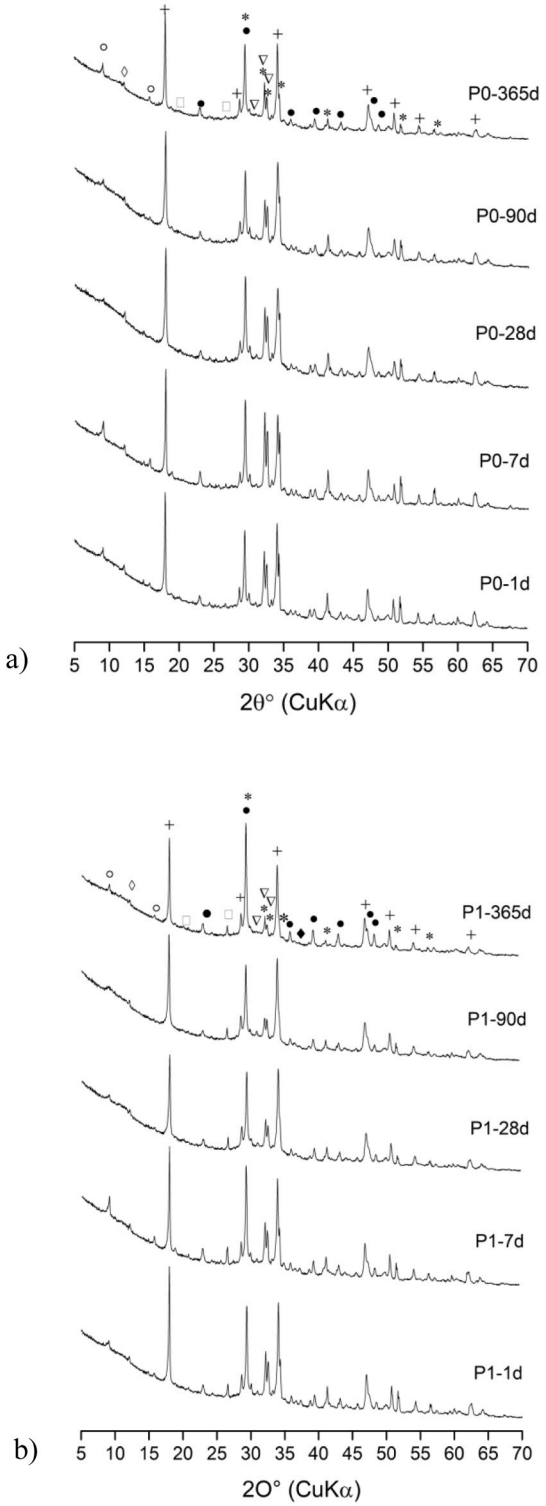

Fig. 5. a) XRD diffractograms of the reference mixture P0 at different sample ages. b) XRD diffractograms of the mixture P1 with WBA at different sample ages. Legend: *=alite, + = portlandite, ○=ettringite, ●=calcite, Δ=belite, ◊=ferrite, □ = quartz, ◆ =lime.

consistent with the thermogravimetric results. More portlandite is present in the samples with WBA addition (also present in unhydrated WBA). A significant decrease in portlandite at 365 days was observed in the WBA mix due to pozzolanic reaction and/or carbonation effects. Even though samples were dried and in between testing sealed in plastic foil and stored in plastic containers, carbonation effect cannot be fully excluded. Ettringite, formed by hydration of the aluminate phase with calcium sulfate, was observed in both samples; however, less was present in samples containing WBA. Calcite was also observed due to carbonation, with higher amounts in the WBA samples as a result of the composition of the raw unhydrated WBA. The amount of calcite varies only slightly over the hydration period, confirming the results of thermogravimetric analysis.

3.4. Evolution of pore microstructure

The pore size distribution (intruded volume) of pastes P0 and P1 at 1, 28, 90 and 365 days is shown in Fig. 6. For the P0 mixture, pore size distribution curve shifts to the left after 1 day of curing, with a decrease in the proportion of larger pores (> 1 μm) and an increase in pores smaller than 0.01 μm (gel pores). This behaviour is characteristic of cement pastes hydration of, as the increase in gel pores is associated with the formation of C−S−H gel [53]. Replacing cement with WBA resulted in a significant proportion of pores ranging from 0.01 to 0.05 μm compared to the reference paste. The proportion of these pores increased with curing time. After 365 days, the pore structures of P0 and P1 overlap corresponding to the mechanical properties of the samples.

In this study, the critical pore entry radius (d_c), threshold pore entry radius (d_{th}), porosity, mean pore diameter and bulk density were determined (Table 6). The critical pore entry radius corresponds to the highest point on the log differential pore volume curve [54]. The critical pore size controls the transmissivity of the material [55]. According to [54], the threshold pore entry radius is the largest pore diameter at which a significant intruded pore volume is detected or where the slope of the cumulative curve increases

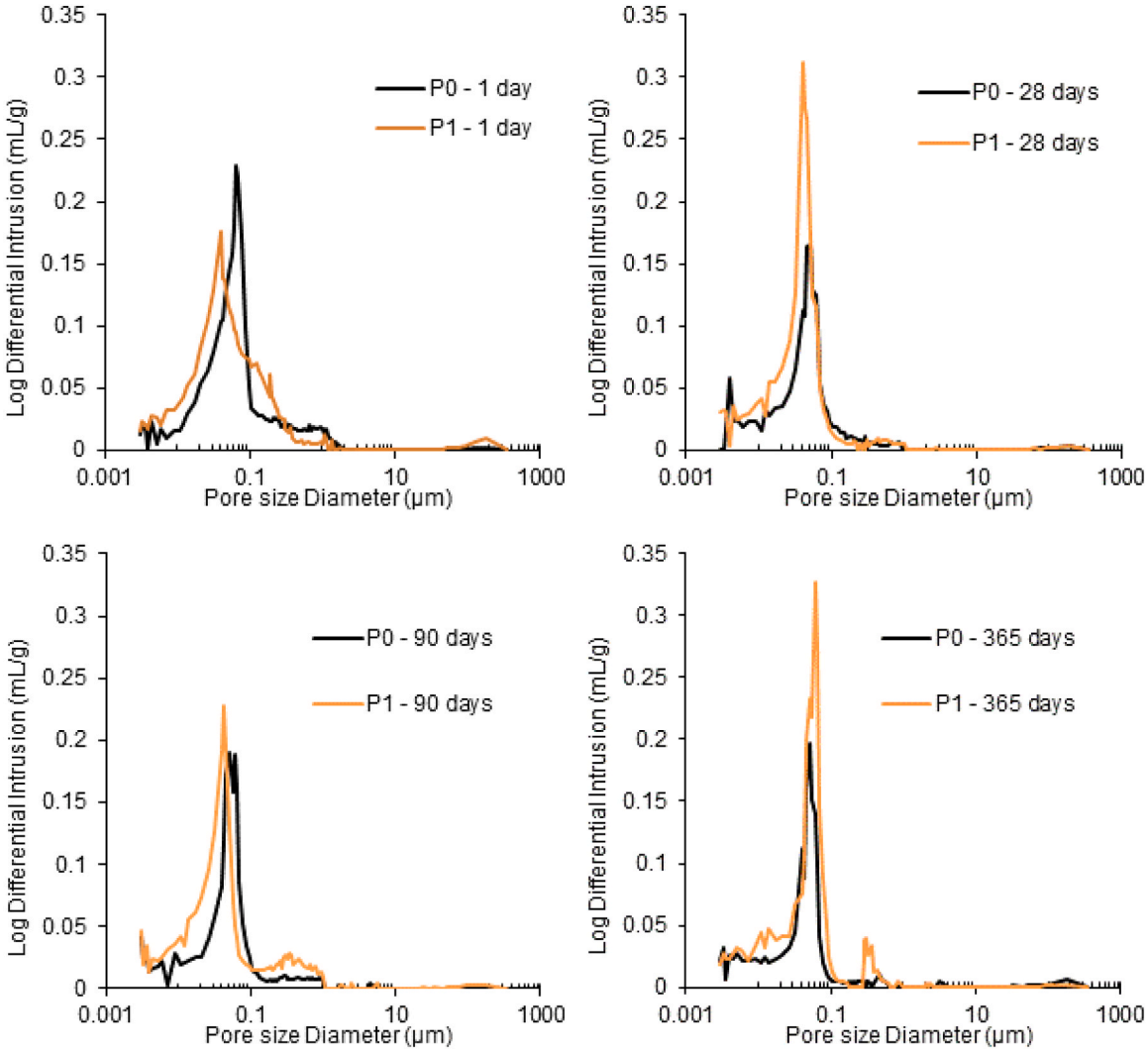

Fig. 6. Pore size distribution (intruded volume) of pastes P0 and P1 at 1, 28, 90, and 365 days, determined by MIP.

abruptly. The values of the critical pore entry radius, representing the most common pore size for sample P0, were larger than in sample P1, but the proportion of these pores was smaller than in sample P1. The same trend was observed for the threshold pore entry radius after 1 day: the threshold pore entry radius was larger for sample P0, possibly indicating that chemical species can penetrate a hardened Portland cement much more easily without WBA [55]. However, during ageing, the threshold pore entry radius values become the same. In general, porosity was higher for all P1 specimens across all observed specimen ages. Over time, porosity decreases in both samples: from 1 to 365 days it is reduced by 8.14% for P0 and by 4.19% for P1.

4. Discussion

Wastes or by-products from other industries, such as slags, coal fly ash, and others used as SCMs, are widely used in the cement and concrete industry. The use of WBAs, their reactivity and their contribution to the mechanical and durability properties of cementitious composites need to be understood. As part of phase III activities of *RILEM TC 267-TRM* [56], the R^3 test (cumulative heat release) and bound water measurement were performed, characterizing WBA as a supplementary cementitious material with low reactivity. The results for R^3 bound water were 2.26 ± 0.34 g/100 g of SCM at 7 days, while the total heat of hydration was 68.5 ± 4.8 J/g of SCM at 3 days and 87.5 ± 5,4 /g of SCM at 7 days. Based on the compressive strength results at 7 days shown in Fig. 3, a similar conclusion can be drawn. The mix with WBA reached only 75% of the compressive strength of the reference mix after one day of curing, which is a larger decrease than would be expected for a completely non-reactive material, considering that only 15% WBA was added. Difference in properties of WBA from pulverised combustion compared to cement could be responsible for a significant early-age strength reduction (21–25% at 7 days) of cement paste and mortar with the addition of WBA,

The results of fresh state properties [8] indicate that the use of WBA delays the setting time and increases the water demand of the paste, which leads to reduced mortar consistency. Based on the chemical, mineralogical and physical properties of WBA as a raw material, the following differences from cement can be identified, all of which may negatively affect water demand and setting: (i) lower density (Table 1) – as mass substitution was used, the mix with 15 wt% of cement replaced by WBA had a larger volume of substituting particles; (ii) higher LOI (Table 1) – a greater amount of organic and unburnt matter, resulting in prolonged setting and increased water requirement; (iii) irregular particle morphology (Fig. 1) – internal voids and a larger surface area to be wetted. All these parameters could negatively affect the water requirement, meaning a greater amount of water is needed to achieve the same workability of the mixture. This increased water content may cause a dilution effect, delaying the hydration reaction and extending the induction period, as shown by the heat of hydration results in Fig. 2. Additionally, the coarser particle size distribution of WBA compared to cement (Fig. 1) may further reduce its reactivity, particularly at early ages. Slower formation of ettringite at 1 day was also observed in the TGA measurement, Fig. 4 and Table 4 (comparison of Δm(m50-m400) for P0 and P1, which are 10.8% and 8.5%, respectively), consequently resulting in slower development of compressive strength, as shown in Fig. 3. Finally, the most prominent impact of higher water demand and coarser particle size of WBA compared to cement, was reflected on the pore structure of the matrix obtained from MIP data. Pore structure results (Table 6) show that the WBA mix (P1) has higher total porosity compared to the reference (P0). Formation of coarser, more porous matrix with WBA addition could be responsible for a significant strength loss of this mix, compared to the reference mix.

In addition to the differences in physical properties of WBA compared to cement, there are certain chemical differences of importance. WBA used had a much higher alkali content than the cement, with 6.60% Na_2O_{eq} compared to 1.67% in the cement (Table 1). When sufficient sulphate is present in the clinker, the alkalis are normally present as sulphates. If there is not enough sulphate in the clinker to obtain the alkalis as their sulphates, the alkalis are assumed to enter the clinker minerals, leading to a change in reactivity [57]. Alkali addition tends to increase the main heat evolution in cements with initially low alkali content, while shortening the induction period in cements with higher alkali content. At the microstructural level, alkalis promote C_3S dissolution and $Ca(OH)_2$ formation, but may inhibit AFt (ettringite) formation [58]. According to the XRD data, these alkalis could possibly form arcanite, K_2SO_4, in WBA (Table 2). According to [59], alkali sulphates, including arcanite, cannot promote 1-day compressive strength and may lead to a decrease in 28-day compressive strength. The increased content of arcanite reduces the formation of ettringite but promotes the formation of C-S-H and portlandite during cement hydration [59].

Results of the strength development, therefore, indicate that the substitution of cement with WBA from pulverised fuel combustion led to a decrease of the early-age strength. However, the strength difference between the P0 and P1, and M0 and M1 mixes decreased

Table 6
Pore parameters (critical pore entry radius, threshold pore entry radius, porosity, and mean pore diameter) and bulk density for pastes P0 and P1 at 1, 28, 90, and 365 days, calculated from the MIP data.

	Critical pore entry radius	Threshold pore entry radius	Porosity	Mean pore diameter	Bulk Density
	μm	μm	%	μm	g/mL
P0–1	0.0659	1.8532	22.92	0.0338	2.4774
P0–28	0.0503	0.9164	16.62	0.0218	2.3742
P0–90	0.0503	0.9842	16.97	0.0227	2.3776
P0–365	0.0503	0.6083	14.78	0.0071	2.3158
P1–1	0.0403	1.1084	24.96	0.0258	2.4379
P1–28	0.0403	0.9951	22.08	0.0208	2.3911
P1–90	0.0431	0.9893	21.28	0.0212	2.3247
P1–365	0.0624	0.9146	20.77	0.0228	2.2860

over time, indicating that the negative impact of WBA on strength development was most pronounced at an early age. Considering the period beyond 7 days, especially the trend in compressive strength development, it is evident that some reactivity is present and that it became dominant only after 7 days. Hypotheses regarding the nature of this reactivity are presented below, supported by the results from the previous chapter.

In the analysis of the heat of hydration behaviour of the samples from Fig. 2, the highest hydration rate occurs within the first 24 h, particularly in sample P0, while sample P1 exhibits a slower initial reaction but achieves a higher cumulative heat after 72 h. Both pastes achieve similar value of cumulative heat at the end of the testing period, regardless of the 15% mass substitution of cement with WBA in the case of paste P1. Therefore, heat flow cannot be attributed solely to the reaction of cement, rather the WBA also contributed to this heat generation, either through physical effects or latent reactivity.

For some SCMs, the increase in heat of hydration can be attributed to the filler effect, i.e. particles smaller than the cement fill spaces and enable higher cement reactivity [60]. The WBA particles were larger than those of the cement, as shown by the PSD (Table 1). Therefore, the filler effect seems unlikely in this case. Some chemical reactivity of WBA is evident, which is significantly slower than that of cement, but still results in heat generation.

The second change in behaviour occurred between 7 and 28 days of curing, when an increase in compressive strength was observed for the WBA mixture (26.6% for the M1 mix). The rate of this increase was more significant than that of the reference mixture, as result of delayed hydration (Fig. 3). One explanation could be that WBA particles act as crystallisation centres around which portlandite and C−S−H begin to crystallise [61]. WBA has a high specific surface area [62], which has been reported to promote the nucleation effect [63]. The enhanced nucleation is associated with fine materials, where the additional surface area provided by the SCMs acts as nucleation sites for the hydration products of the clinker phases [2]. Another hypothesis is the pozzolanic reaction of WBA with portlandite to form aluminate phases, such as AFm ($3CaO{\cdot}Al_2O_3{\cdot}Ca(OH)_2{\cdot}x\ H_2O$), and/or C−S−H. The study by Ukrainczyk et al. [32] on the hydration of WBA alone showed that the ash contains reactive aluminate phases, namely brownmillerite and gehlenite ($2CaO{\cdot}Al_2O_3{\cdot}SiO_2$), which contribute to a pozzolanic reaction that reduces the content of the most soluble $Ca(OH)_2$. Moreover, the formation of the very stable (desirable and durable) hydration product strätlingite was also confirmed, the origin of which can be attributed to the combined hydration of belite ($2CaO{\cdot}SiO_2$), aluminoferrite ($4CaO{\cdot}Al_2Fe_2O_6$) and gehlenite ($2CaO{\cdot}Al_2O_3{\cdot}SiO_2$). To test this hypothesis, the amounts of bound water and portlandite were evaluated from the mass losses at different temperatures. Estimating of the amount of portlandite (CH) as a hydration product is used to assess the degree of hydration of a paste and indicates its possible influence on the mechanical properties after curing. The influence of WBA as a partial replacement of cement on the bound water (H) and the amount of portlandite (CH), as determined by TG analysis, is shown in 7 a) and b).

At the beginning of hydration, the mixture with WBA produced a slightly higher amount of $Ca(OH)_2$ than the reference mixture. This can be attributed to both the presence of portlandite as a mineral phase (26.6 wt%) in WBA and the hydraulic properties of the ash, which contains a relatively high amount of reactive CaO (13.5 wt%). After 28 days, there was a discrete trend of portlandite decrease (for 2 wt%). Since this decrease is not followed by the increase in the amount of calcite, a decrease in portlandite cannot be attributed to carbonation, but rather to the delayed pozzolanic reaction [64,65]. A similar decrease in portlandite values due to the pozzolanic reaction has been observed in the previous studies. According to the study presented in [22], the addition of 30% WBA as a cement replacement resulted in the decrease in the amount of portlandite compared to the ash-free cement composite, which was also observed with this WBA. The study by [32] investigated the consumption of portlandite in specimens where only WBA was used as a binder. The results showed the maximum amount of portlandite at 3 days, which gradually decreased with ageing. The authors [32] reported that after 28 days the amount of portlandite was lower, which was attributed to the pozzolanic activity of WBA and/or the activation of pozzolanic additives in the cement (CEM II/A-M (S-V) 42.5 N) used in the mixes. After 365 days, the amount of portlandite in the P0 sample increased slightly, while in the P1 sample it decreased more significantly. According to the values in Table 5, for P1 sample portlandite decreased from 21.3% at 90 days to 15.5.% at 365 days, while calcite increased from 14.4.% at 90 days to 20.1% at 365 days. Therefore, this decrease in portlandite at 365 days for P1 mix can be attributed to carbonation occurring over the course of one year. In cementitious system with lower amount of available portlandite, C-S-H undergoes carbonation, leading to the formation of calcium carbonate and a silica gel-like product [66]. This amorphous silica (silica gel) increases reactivity and contributes to the pozzolanic reaction of carbonated samples. This could also be the case in P1 sample after 365 days, where an increase of compressive strength could be attributed to the complementary process of pozzolanic reaction and carbonation.

Next, the evolution of bound water can be analysed (Fig. 7b). In the reference mixture, a significant amount of bound water was present after 7 days of curing. This bound water was attributed to the development of C−S−H and ettringite in the cement mixture, which is associated with a significant increase in compressive strength. For the WBA mixture (P1), the amount of bound water after 7 days was lower than in the reference mixture (P0), which is consistent with the lower compressive strength at this age. However, between 7 and 28 days of curing, there was a significant increase in bound water for the WBA mixture, while the reference mixture showed a decrease in bound water content. The decrease in bound water for the P0 mixture could be attributed to carbonation, as an increase in mass loss was also observed for this mixture between 600 and 950 °C. For the WBA mixture, an increase in bound water can be attributed to the formation of hydration products, which in turn correlates with an increase in compressive strength. After 28 days, the WBA mix exhibited a sharp decrease in the amount of bound water, which correlates with the increase in mass loss between 600 and 950 ° and can thus be attributed to carbonation. This sharp drop highlights the particular importance of the storage conditions of the samples but also indicates the potential for CO_2 storage [67,68].

Another indication of the reactivity of WBA after 7 days is seen in the evolution of the pore size distribution. Fig. 8 presents the distribution of pores in the following ranges: gel pores (< 0.01 μm), medium capillaries (0.01 – 0.05 μm), large capillaries (0.05 – 1 μm) and large capillaries and entrained air (> 1 μm) according to [69]. Between 1 and 28 days, a clear increase in gel pores and medium capillaries is clearly observed in the WBA mixture. As stated before, during early age the MIP data shows that the WBA mix (P1) has

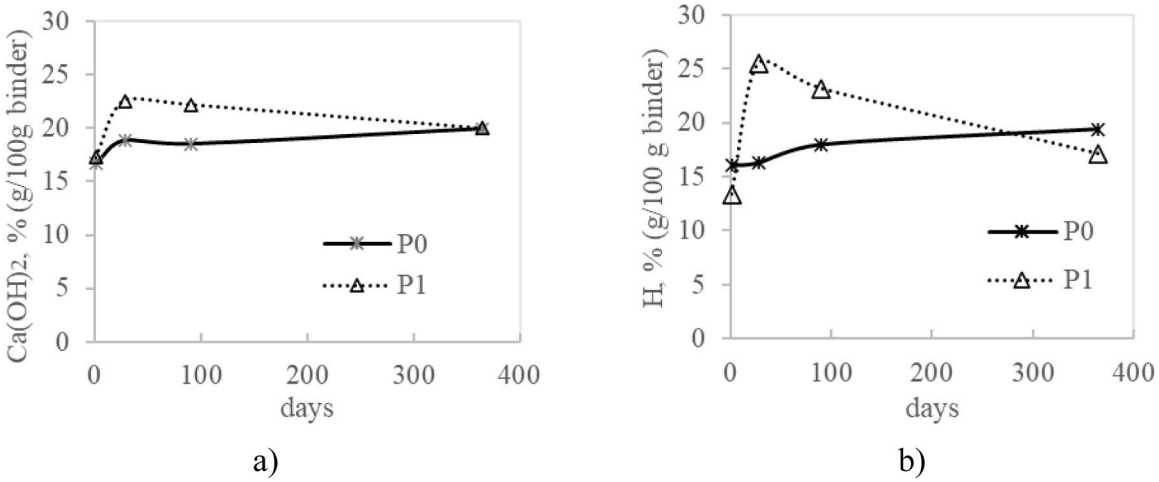

Fig. 7. a) Portlandite content; b) Bound water content.

higher total porosity and a larger volume of medium capillaries (0.01–0.05 μm), which could be the primary cause of strength loss of P1 mix at early age. However, at later ages, there is evident refinement of the pore size distribution in the case of P1, which may be associated with the formation of hydration products and carbonates at later ages. The results further strengthen the hypothesis that the long-term performance is governed by a slow pozzolanic reaction of WBA from pulverised fuel combustion and carbonation of cementitious matrix, both causing densifying of the microstructure and te increase in compressive strength at later ages.

5. Conclusions

In this study, as-collected fly WBA from a pulverised fuel combustor was used as a cement replacement to investigate the long-term effect of WBA on the microstructure of cement composites. Replacing cement with 15% WBA caused a higher water demand and a dilution effect, leading to a delay in the hydration reaction, prolongation of the induction period in the hydration kinetics, and lower early mechanical properties. Evaluation of the pore structure showed that replacing cement with WBA resulted in a significant increase in the amount of medium capillary pores (0.01–0.05 μm). Results presented confirm that the dominant early-age effect of WBA from pulverised fuel combustion is physical (water demand, dilution) leading to a porous microstructure and strength loss.

Although replacing cement with WBA initially reduces compressive strength, over time samples with WBA exhibit mechanical performance comparable to the reference samples. The time-dependent evolution of bound water and portlandite in cement pastes, determined by TGA, showed a slow pozzolanic response and calcite formation, both correlating with increased compressive strength at later ages. Therefore, results presented confirm that the long-term performance of composite with WBA from pulverised fuel combustion is governed by slow chemical processes, namely a pozzolanic reaction consuming portlandite and carbonation, which together densify the microstructure by increasing gel pores.

Understanding the effect of WBA from pulverised fuel combustion on the properties of cementitious composites at early age and

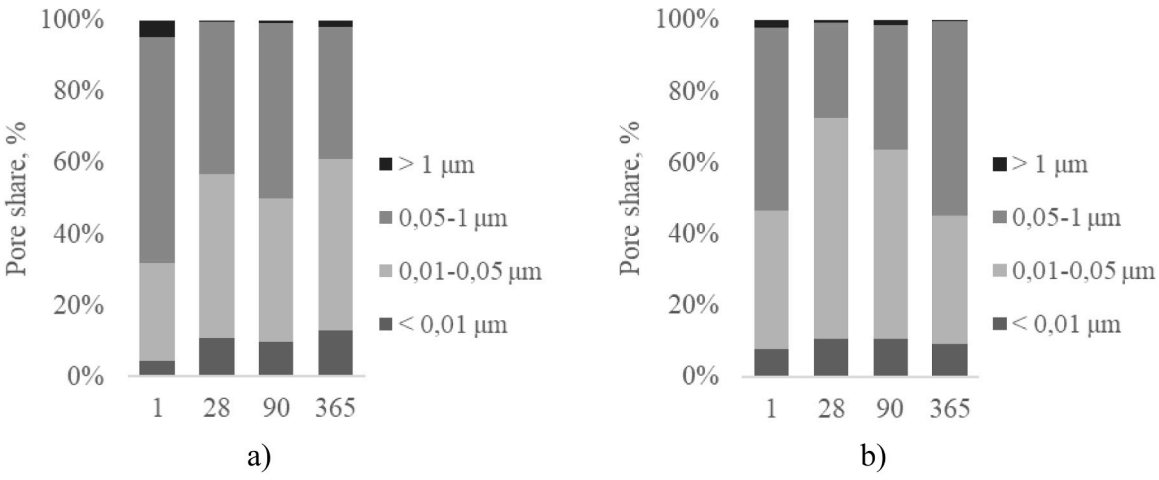

Fig. 8. Pore size distribution (pore share) after 1, 28, 90 and 365 days for: a) paste P0 and b) paste P1, obtained from MIP data.

over longer curing periods contributes to optimising their use and replacement levels in blended systems. The extensive experimental results presented in this study confirm the potential of WBA from pulverised fuel combustion as a cement substitute. For further optimisation and tailoring for use in concrete applications, the durability of cementitious composites with WBA from pulverised fuel combustion should be assessed across various environments.

CRediT authorship contribution statement

Ivana Carević: Writing – original draft, Methodology, Investigation, Data curation. **Marijana Serdar:** Writing – review & editing, Validation, Methodology. **Maruša Mrak:** Writing – review & editing, Investigation, Data curation. **Nina Štirmer:** Writing – review & editing, Supervision, Project administration, Funding acquisition. **Vilma Ducman:** Writing – review & editing, Methodology, Conceptualization. **Sabina Dolenec:** Writing – review & editing, Investigation.

Declaration Of Competing Interest

The authors declare that they have no known competing financial interests or personal relationships that could have appeared to influence the work reported in this paper.

Acknowledgements

This research was conducted within the framework of the research project AshCycle – Integration of Underutilized Ashes into Material Cycles by Industry-Urban Symbiosis (Project No. 101058162), funded under HORIZON-CL4–2021-TWIN-TRANSITION−01. The authors would like to thank the institutional project of the University of Zagreb Faculty of Civil Engineering, *LCEFORCE – Integrated Application of Life Cycle Engineering in the Construction Sector* which was co-financed by funds from the National Recovery and Resilience Plan 2021–2026 and the HORIZON project ASCCENT – Active storage of captured CO_2 in net zero construction products (ID: 101159895).

Data availability

Data will be made available on request.

References

[1] D. Ndahirwa, H. Zmamou, H. Lenormand, N. Leblanc, The role of supplementary cementitious materials in hydration, durability and shrinkage of cement-based materials, their environmental and economic benefits: a review, Clean. Mater. 5 (2022) 100123, https://doi.org/10.1016/j.clema.2022.100123.
[2] B. Lothenbach, K. Scrivener, R.D. Hooton, Supplementary cementitious materials, Cem. Concr. Res. 41 (2011) 1244–1256, https://doi.org/10.1016/j.cemconres.2010.12.001.
[3] K.L. Scrivener, P. Juilland, P.J.M. Monteiro, Advances in understanding hydration of Portland cement, Cem. Concr. Res. 78 (2015) 38–56, https://doi.org/10.1016/j.cemconres.2015.05.025.
[4] J. Zhou, G. Ye, K. van Breugel, Characterization of pore structure in cement-based materials using pressurization-depressurization cycling mercury intrusion porosimetry (PDC-MIP), Cem. Concr. Res. 40 (2010) 1120–1128, https://doi.org/10.1016/j.cemconres.2010.02.011.
[5] E.M.J. Berodier, Impact of the supplementary cementitious materials on the kinetics and microstructural development of cement hydration, Dr. Thesis 417 Éc. Polytech. Fed. De. Lausanne Switz. (2015).
[6] X. Liang, Z. Li, H. Dong, G. Ye, review on the characteristics of wood biomass fly ash and their influences on the valorization in cementitious materials, J. Build. Eng. 97 (2024) 110927, https://doi.org/10.1016/j.jobe.2024.110927.
[7] Y. Vanhove, J.G. Dossa, J. Page, C. Djelal, Rheological benefits of biomass fly ash as filler replacement in cement-based materials, Case Stud. Constr. Mater. 22 (2025) e04133, https://doi.org/10.1016/j.cscm.2024.e04133.
[8] I. Carević, A. Baričević, N. Štirmer, J. Šantek Bajto, Correlation between physical and chemical properties of wood biomass ash and cement composites performances, Constr. Build. Mater. 256 (2020) 119450, https://doi.org/10.1016/j.conbuildmat.2020.119450.
[9] F. Bülbül, L. Courard, Turning waste into greener cementitious building material: treatment methods for biomass ashes - a review, Materials 18 (2025) 834, https://doi.org/10.3390/ma18040834.
[10] Y. Yang, K. Takasu, H. Suyama, X. Ji, M. Xu, Z. Liu, Comparative analysis of woody biomass fly ash and Class F Fly ash as supplementary cementitious materials in mortar, Materials 17 (2024) 3723, https://doi.org/10.3390/ma17153723.
[11] M. Salvo, S. Rizzo, M. Caldirola, G. Novajra, F. Canonico, M. Bianchi, M. Ferraris, Biomass ash as supplementary cementitious material (SCM), Adv. Appl. Ceram. 114 (2015) 3–10, https://doi.org/10.1179/1743676115Y.0000000043.
[12] S. Demis, J.G. Tapali, V.G. Papadakis, An investigation of the effectiveness of the utilization of biomass ashes as pozzolanic materials, Constr. Build. Mater. 68 (2014) 291–300, https://doi.org/10.1016/j.conbuildmat.2014.06.071.
[13] L.R. Caldas, M.Y.R. Da Gloria, F. Pittau, V.M. Andreola, G. Habert, R.D. Toledo Filho, Environmental impact assessment of wood bio-concretes: Evaluation of the influence of different supplementary cementitious materials, Constr. Build. Mater. 268 (2021) 121146, https://doi.org/10.1016/j.conbuildmat.2020.121146.
[14] A.B. Ayobami, Performance of wood bottom ash in cement-based applications and comparison with other selected ashes: overview, Resour. Conserv. Recycl. 166 (2021) 105351, https://doi.org/10.1016/j.resconrec.2020.105351.
[15] O. Lescinskis, A. Sapata, G. Bumanis, M. Sinka, X. Zhou, D. Bajare, The potential of wood ash to be used as a supplementary cementitious material in cement mortars, Buildings 15 (9) (2025) 1507, https://doi.org/10.3390/buildings15091507.
[16] E. Pandolfi Balbi, P. Comodi, C. Cambi, M. Fastelli, A. Corradini, C. Montanari, A. Zucchini, G. Cerni, H. Bou Farhat, C. Bocci, R. Snellings, Wood biomass ash, municipal solid waste ash, and recycled concrete from construction demolition waste as supplementary cementitious materials in fine graded granular mixtures, Constr. Build. Mater. 498 (2025) 144016, https://doi.org/10.1016/j.conbuildmat.2025.144016.
[17] E.E. Teker Ercan, L. Andreas, A. Cwirzen, K. Habermehl-Cwirzen, Ground wood ash as a supplementary cementitious material: effects on strength, durability and environmental performance of concrete, Constr. Build. Mater. 503 (2025) 144520, https://doi.org/10.1016/j.conbuildmat.2025.144520.
[18] I. Carević, M. Serdar, N. Štirmer, N. Ukrainczyk, Preliminary screening of wood biomass ashes for partial resources replacements in cementitious materials, J. Clean. Prod. 229 (2019) 1045–1064, https://doi.org/10.1016/j.jclepro.2019.04.321.

[19] N.M. Sigvardsen, G.M. Kirkelund, P.E. Jensen, M.R. Geiker, L.M. Ottosen, Impact of production parameters on physiochemical characteristics of wood ash for possible utilisation in cement-based materials, Resour. Conserv. Recycl. 145 (2019) 230–240, https://doi.org/10.1016/j.resconrec.2019.02.034.
[20] K. Kostanić Jurić, I. Carević, M. Serdar, N. Štirmer, Feasibility of using pozzolanicity tests to assess reactivity of wood biomass fly ashes, Gradjevinar 72 (2021) 1145–1153, https://doi.org/10.14256/JCE.2950.2020.
[21] T. Ramos, A.M. Matos, J. Sousa-Coutinho, Mortar with wood waste ash: mechanical strength carbonation resistance and ASR expansion, Constr. Build. Mater. 49 (2013) 343–351, https://doi.org/10.1016/j.conbuildmat.2013.08.026.
[22] R. Rajamma, R.J. Ball, L.A.C. Tarelho, G.C. Allen, J.A. Labrincha, V.M. Ferreira, Characterisation and use of biomass fly ash in cement-based materials, J. Hazard. Mater. 172 (2009) 1049–1060, https://doi.org/10.1016/j.jhazmat.2009.07.109.
[23] S. Kramar, V. Ducman, Evaluation of ash pozzolanic activity by means of the strength activity index test, Frattini test and DTA/TG analysis, Tehnicki Vjesnik 25 (2018) 1746–1752, https://doi.org/10.17559/TV-20171203193229.
[24] N.M. Sigvardsen, M.R. Geiker, L.M. Ottosen, Phase development and mechanical response of low-level cement replacements with wood ash and washed wood ash, Constr. Build. Mater. 269 (2021) 121234, https://doi.org/10.1016/j.conbuildmat.2020.121234.
[25] V.A. Vu, A. Cloutier, B. Bissonnette, P. Blanchet, J. Duchesne, The effect of wood ash as a partial cement replacement material for making wood-cement panels, Materials 12 (17) (2019) 2766, https://doi.org/10.3390/ma12172766.
[26] N.M. Sigvardsen, M.R. Geiker, L.M. Ottosen, Reaction mechanisms of wood ash for use as a partial cement replacement, Constr. Build. Mater. 286 (2021) 122889, https://doi.org/10.1016/j.conbuildmat.2021.122889.
[27] K. Ohenoja, P. Tanskanen, V. Wigren, P. Kinnunen, M. Körkkö, O. Peltosaari, J. Österbacka, M. Illikainen, Self-hardening of fly ashes from a bubbling fluidized bed combustion of peat, forest industry residuals, and wastes, Fuel 165 (2016) 440–446, https://doi.org/10.1016/j.fuel.2015.10.093.
[28] A. Danish, O. Karadag, T. Bilir, T. Ozbakkaloglu, Valorization of biomass ashes in the production of cementitious composites: a comprehensive review of properties and performance, Constr. Build. Mater. 405 (2023) 133244, https://doi.org/10.1016/j.conbuildmat.2023.133244.
[29] I. Carević, J.Šantek Bajto, M. Grubor, N. Štirmer, Wood biomass ash as a clinker substitute in advancing next-generation blended cement: Croatian case study, Sci. Rep. 16 (2026) 3932, https://doi.org/10.1038/s41598-025-33867-x.
[30] G. Fava, T.R. Naik, M. Pierpaoli, Compressive strength and leaching behavior of mortars with biomass ash, Recycling 3 (3) (2018) 46, https://doi.org/10.3390/recycling3030046.
[31] S. Maschio, G. Tonello, L. Piani, E. Furlani, Fly and bottom ashes from biomass combustion as cement replacing components in mortars production: rheological behaviour of the pastes and materials compression strength, Chemosphere 85 (2011) 666–671, https://doi.org/10.1016/j.chemosphere.2011.06.070.
[32] N. Ukrainczyk, N. Vrbos, EAB. Koenders, Reuse of woody biomass ash waste in cementitious materials, Chem. Biochem. Eng. Q 30 (2016) 137–148, https://doi.org/10.15255/CABEQ.2015.2231.
[33] J.M. Medina, I.F. Sáez del Bosque, M. Frías, M.I. Sánchez de Rojas, C. Medina, Durability of new blended cements additioned with recycled biomass bottom ASH from electric power plants, Constr. Build. Mater. 225 (2019) 429–440, https://doi.org/10.1016/j.conbuildmat.2019.07.176.
[34] S. Pachchigar, M.D.B. Takehara, E. Pettersson, M. Öhman, Ash Transformation Processes during Pulverized Fuel Combustion of Rice Husks, Energy Fuels 39 (2025) 4481–4493, https://doi.org/10.1021/acs.energyfuels.4c05412.
[35] M. Dal Belo Takehara, K. Umeki, R. Gebart, Investigation of oxygen-enriched biomass flames in a lab-scale entrained flow reactor, Fuel 366 (2024) 131343, https://doi.org/10.1016/j.fuel.2024.131343.
[36] The European Committee for Standardization. Solid biofuels – Determination of major elements – Al, Ca, Fe, Mg, P, K, Si, Na i Ti (ISO 16967:2015; EN ISO 16967:2015) 2015.
[37] The European Committee for Standardization, Charact. Sludge – Determ. pH-Value (EN 12176 (1998) 1998.
[38] ASTM International. ASTM D 7348-13 Standard Test Methods for Loss on Ignition (LOI) of Solid Combustion Residues, 2013.
[39] ASTM International. ASTM C188-17, Standard Test Method for Density of Hydraulic Cement, 2017.
[40] The European Committee for Standardization EN 451-1 Method of testing fly ash – Part 1: Determination of free calcium oxide content, 2017.
[41] The European Committee for Standardization EN 196-3:: Methods of testing cement – Part 3: Determination of setting times and soundness, 2016.
[42] The European Committee for Standardization EN 196-1: Methods of testing cement – Part 1: Determination of strength, 1996.
[43] Lidija Korat Bensa. Characterization of Cement Composites with Mineral Additives, Doctoral thesis (in Slovenian). Faculty of Civil and Geodetic Engineering, University of Ljubljana, Slovenia, 2015.
[44] K. Scrivener, R. Snellings, B. Lothenbach. A Practical Guide to Microstructural Analysis of Cementitious Materials, 1st ed, Boca Raton: CRC Press, 2018.
[45] F. Deschner, F. Winnefeld, B. Lothenbach, S. Seufert, P. Schwesig, S. Dittrich, F. Goetz-Neunhoeffer, J. Neubauer, Hydration of Portland cement with high replacement by siliceous fly ash, Cem. Concr. Res. 42 (2012) 1389–1400, https://doi.org/10.1016/j.cemconres.2012.06.009.
[46] N. Ukrainczyk, M. Ukrainczyk, J. Šipušić, T. Matusinović, XRD and TGA investigation of hardened cement paste degradation. MATRIB 2006 International Conference on Materials, Tribology, Recycling, 2006, pp. 22–24.
[47] K.W. Kim, K.T. Park, F. Ates, H.G. Kim, B.H. Woo, Effect of pretreated biomass fly ash on the mechanical properties and durability of cement mortar, Case Stud. Constr. Mater. 18 (2023) e01754, https://doi.org/10.1016/j.cscm.2022.e01754.
[48] I. Gabrijel, M. Skazlić, N. Štirmer, Long-term behavior of concrete containing wood biomass fly ash, Appl. Sci. 12 (24) (2022) 12859, https://doi.org/10.3390/app122412859.
[49] W. Deboucha, N. Leklou, A. Khelidj, M.N. Oudjit, Hydration development of mineral additives blended cement using thermogravimetric analysis (TGA): methodology of calculating the degree of hydration, Constr. Build. Mater. 146 (2017) 687–701, https://doi.org/10.1016/j.conbuildmat.2017.04.132.
[50] E.T. Stepkowska, J.M. Blanes, F. Franco, C. Real, JL. Pérez-Rodríguez, Phase transformation on heating of an aged cement paste, Thermochim. Acta 420 (2004) 79–87, https://doi.org/10.1016/j.tca.2003.11.057.
[51] A. Morandeau, M. Thiéry, P. Dangla, Investigation of the carbonation mechanism of CH and C-S-H in terms of kinetics, microstructure changes and moisture properties, Cem. Concr. Res. 56 (2014) 153–170, https://doi.org/10.1016/j.cemconres.2013.11.015.
[52] P. Nielsen, M. Quaghebeur, Determination of the CO2 uptake of construction products manufactured by mineral carbonation, Minerals 13 (8) (2023) 1079, https://doi.org/10.3390/min13081079.
[53] H.M. Jennings, Design of high strength cement based materials: Part 2 microstructure, Mater. Sci. Technol. 4 (4) (1988) 285–290, https://doi.org/10.1179/mst.1988.4.4.285.
[54] H. Ma, Mercury intrusion porosimetry in concrete technology: tips in measurement, pore structure parameter acquisition and application, J. Porous Mater. 21 (2014) 207–215, https://doi.org/10.1007/s10934-013-9765-4.
[55] P. Pipilikaki, M. Beazi-Katsioti, The assessment of porosity and pore size distribution of limestone Portland cement pastes, Constr. Build. Mater. 23 (2009) 1966–1970, https://doi.org/10.1016/j.conbuildmat.2008.08.028.
[56] X. Li, R. Snellings, M. Antoni, N.M. Alderete, M. Ben Haha, S. Bishnoi, et al., Reactivity tests for supplementary cementitious materials: RILEM TC 267-TRM phase 1, Mater. Struct. /Mater. Constr. 51 (2018) 151, https://doi.org/10.1617/s11527-018-1269-x.
[57] I. Jawed, J. Skalny, Alkalies in cement: a review I. Forms of Alkalies and Their Effect on Clinker Formation, Pergamon Press. Inc. 7 (1977).
[58] L. Huang, P. Yan, Effect of alkali content in cement on its hydration kinetics and mechanical properties, Constr. Build. Mater. 228 (2019) 116833, https://doi.org/10.1016/j.conbuildmat.2019.116833.
[59] Y. Ma, J. Qian, Influence of alkali sulfates in clinker on the hydration and hardening of Portland cement, Constr. Build. Mater. 180 (2018) 351–363, https://doi.org/10.1016/j.conbuildmat.2018.05.196.
[60] J. Skibsted, R. Snellings, Reactivity of supplementary cementitious materials (SCMs) in cement blends, Cem. Concr. Res. 124 (2019) 105799, https://doi.org/10.1016/j.cemconres.2019.105799.
[61] R. Kaminskas, V. Cesnauskas, Influence of activated biomass fly ash on portland cement hydration, Ceram. Silik. áty 58 (4) (2014) 260–268.
[62] C.B. Cheah, M. Ramli, The fluid transport properties of HCWA-DSF hybrid supplementary binder mortar, Compos. B. Eng. 56 (2014) 681–690, https://doi.org/10.1016/j.compositesb.2013.09.021.

[63] J. Rissanen, K. Ohenoja, P. Kinnunen, M. Illikainen, Partial replacement of portland-composite cement by fluidized bed combustion fly ash, J. Mater. Civ. Eng. 29 (2017) 04017061, https://doi.org/10.1061/(asce)mt.1943-5533.0001899.
[64] K. De Weerdt, M.Ben Haha, G. Le Saout, K.O. Kjellsen, H. Justnes, B. Lothenbach, Hydration mechanisms of ternary Portland cements containing limestone powder and fly ash, Cem. Concr. Res. 41 (2011) 279–291, https://doi.org/10.1016/j.cemconres.2010.11.014.
[65] K.L. Scrivener, B. Lothenbach, N. De Belie, E. Gruyaert, J. Skibsted, R. Snellings, A. Vollpracht, TC 238-SCM: hydration and microstructure of concrete with SCMs: state of the art on methods to determine degree of reaction of SCMs, Mater. Struct. /Mater. Constr. 48 (2015) 835–862, https://doi.org/10.1617/s11527-015-0527-4.
[66] B. Lu, Z. Huo, Q. Xu, G. Hou, X. Wang, J. Liu, H. X, Characteristics of CSH under carbonation and its effects on the hydration and microstructure of cement paste, Constr. Build. Mater. 364 (2023) 129952, https://doi.org/10.1016/j.conbuildmat.2022.129952.
[67] N. Kavčič, S. Tominc, L. Žibret, G. Žibret, M. Kolar, V. Ducman, Comparing methods for determining the CO2content in CO2-Sequestering materials and natural rock, Ceram. Int. 51 (2025) 43786–43795, https://doi.org/10.1016/j.ceramint.2025.07.109.
[68] S. Tominc, M. Pavlin, L. Žibret, V. Ducman, L.M. Ottosen, Sequestration capacity of bio-based ashes and influence of carbonation on the leaching behavior depending on their mineralogical composition, Ceram. Int. 51 (2025) 65512–65523, https://doi.org/10.1016/j.ceramint.2025.11.229.
[69] D.A. Silva, V.M. John, J.L.D. Ribeiro, H.R. Roman, Pore size distribution of hydrated cement pastes modified with polymers, Cem. Concr. Res. 31 (8) (2001) 1177–1184, https://doi.org/10.1016/S0008-8846(01)00549-X.